HHS Public Access

Author manuscript

Int J Radiat Oncol Biol Phys. Author manuscript; available in PMC 2023 March 15.

Published in final edited form as:

Int J Radiat Oncol Biol Phys. 2022 March 15; 112(4): 951–963. doi:10.1016/j.ijrobp.2021.10.146.

Longitudinal Preclinical Imaging Characterizes Extracellular Drug Accumulation After Radiation Therapy in the Healthy and Leukemic Bone Marrow Vascular Microenvironment

Jamison Brooks, PhD[*,†], **Darren Zuro, PhD**[*,†], **Joo Y. Song, MD**[‡], **Srideshikan Sargur Madabushi, PhD**[*], **James F. Sanchez, PhD**[§], **Chandan Guha, MBBS, PhD**[‖], **Marcin Kortylewski, PhD**[#], **Bihong T. Chen, MD, PhD**[**], **Kalpna Gupta, PhD**[††,‡‡], **Guy Storme, MD, PhD**[§§], **Jerry Froelich, MD**[‖ ‖], **Susanta K Hui, PhD**[*,§]

[*]Department of Radiation Oncology, City of Hope, Duarte, California

[†]Department of Radiation Oncology, University of Minnesota, Minneapolis, Minnesota

[‡]Department of Pathology, City of Hope, Duarte, California

[§]Beckman Research Institute of City of Hope, Duarte, California

[‖]Department of Radiation Oncology, Albert Einstein College of Medicine, Montefiore Medical Center, Bronx, New York

[#]Department of Immuno-Oncology, Beckman Research Institute, City of Hope, Duarte, California

[**]Department of Diagnostic Radiology, City of Hope Medical Center, Duarte, California

[††]Hematology/Oncology, Department of Medicine, University of California, Irvine and Southern California Institute for Research and Education, VA Medical Center, North Hills, California

[‡‡]Division of Hematology, Oncology and Transplantation, Department of Medicine, University of Minnesota, Minneapolis, Minnesota

[§§]Department of Radiotherapy, UZ Brussel, Jette, Belgium

[‖ ‖]Department of Radiology, University of Minnesota, Minneapolis, Minnesota

Abstract

Purpose: Recent initial findings suggest that radiation therapy improves blood perfusion and cellular chemotherapy uptake in mice with leukemia. However, the ability of radiation therapy to influence drug accumulation in the extracellular bone marrow tissue is unknown, due in part to a lack of methodology. This study developed longitudinal quantitative multiphoton microscopy (L-QMPM) to characterize the bone marrow vasculature (BMV) and drug accumulation in the extracellular bone marrow tissue before and after radiation therapy in mice bearing leukemia.

Methods and Materials: We developed a longitudinal window implant for L-QMPM imaging of the calvarium BMV before, 2 days after, and 5 days after total body irradiation (TBI). Live

Corresponding author: Susanta K. Hui, PhD, shui@coh.org.

Research data are stored in an institutional repository and will be shared upon reasonable request to the corresponding author.

Supplementary material associated with this article can be found, in the online version, at doi:10.1016/j.ijrobp.2021.10.146.

time-lapsed images of a fluorescent drug surrogate were used to obtain measurements, including tissue wash-in slope (WIS_{tissue}) to measure extracellular drug accumulation. We performed L-QMPM imaging on healthy C57BL/6 (WT) mice, as well as mice bearing acute lymphoblastic leukemia (ALL) and acute myeloid leukemia (AML).

Results: Implants had no effects on calvarium dose, and parameters for wild-type untreated mice were stable during imaging. We observed decreased vessel diameter, vessel blood flow, and WIS_{tissue} with the onset of AML and ALL. Two to 10 Gy TBI increased WIS_{tissue} and vessel diameter 2 days after radiation therapy in all 3 groups of mice and increased single-vessel blood flow in mice bearing ALL and AML. Increased WIS_{tissue} was observed 5 days after 10 Gy TBI or 4 Gy split-dose TBI (2 treatments of 2 Gy spaced 3 days apart).

Conclusions: L-QMPM provides stable functional assessments of the BMV. Nonmyeloablative and myeloablative TBI increases extracellular drug accumulation in the leukemic bone marrow 2 to 5 days posttreatment, likely through improved blood perfusion and drug exchange from the BMV to the extravascular tissue. Our data show that neo-adjuvant TBI at doses from 2 Gy to 10 Gy conditions the BMV to improve drug transport to the bone marrow.

Introduction

It has been shown that leukemia-induced bone marrow vasculature (BMV) remodeling promotes chemoresistance in mice bearing acute myeloid leukemia (AML).[1,2] Angiogenesis is commonly observed in patients with leukemia,[3] and murine studies using human AML have reported vascular alterations that result in poor drug tissue perfusion, similarly to solid tumor models.[4] Despite such observations, antiangiogenic therapeutic approaches in combination with standard chemotherapy have not been successful in improving patient outcomes for leukemia.[5,6] This may in part be due to the complex response of the vascular system to treatment as well as a lack of methods to assess the function of the BMV.[7]

One technique to assess the function of the BMV is dynamic contrast-enhanced (DCE) imaging with modalities such as magnetic resonance imaging (MRI) or computed tomography (CT). DCE imaging acquires time-lapsed images of intravenously injected contrast agents to quantify changes in their delivery to the tissue.[8] However, DCE imaging is unable to directly observe the underlying vascular characteristics influencing changes in contrast delivery.[9] DCE imaging using a small molecular weight contrast agent (938 Da) has revealed increased peak height and wash-in slope in the bone marrow of patients with AML compared with healthy volunteers.[10] Increased blood perfusion and blood volume have been proposed as reasons for changes in peak height and wash-in slope, respectively. Other studies have noticed increased clearance rates of compounds from the bone marrow of patients with acute leukemias[11]; however, the results of these experiments are very different from previously mentioned preclinical observations of poor chemotherapy delivery with the onset of leukemia. Such apparent differences between preclinical and clinical observations demonstrate the need for preclinical methodology capable of performing clinically relevant contrast-based time-lapsed imaging while directly observing BMV alterations.

Multiphoton microscopy is one imaging technique capable of both directly observing the BMV and performing contrast-based time-lapsed imaging. Fluorescent dextran conjugates of

a variety of molecular weights are commonly used for multiphoton microscopy as a contrast agent. Leakage of dextran with molecular weights up to 150 kDa have been observed in the bone marrow[1,12] owing to the presence of highly permeable sinusoidal vessels.[13] In comparison to 150 kDa sized dextran, 4 kDa sized dextran easily permeates the BMV and is similar in molecular weight to typical chemotherapies used in the treatment of leukemia, such as daunorubicin (563.98 Da) or cytarabine (243.22 Da).[14] It is also similar in size to previously mentioned contrast agents used in DCE imaging. Compared with chemotherapy, 4 kDa dextran has a minimal effect on the bone marrow microenvironment,[15] making it ideal for longitudinal studies as a drug surrogate and useful for comparison with DCE imaging.

Using multiphoton microscopy, we recently found that low dose (2–4 Gy) radiation therapy increases single-vessel blood flow in mice bearing acute lymphoblastic leukemia (ALL).[12] Increases in perfusion coincided with increased cellular uptake of chemotherapy, as well as improved survival outcome for mice treated with chemotherapy after neo-adjuvant low-dose radiation therapy. The results suggest that improved BMV blood flow may improve drug accumulation in the extracellular bone marrow tissue, leading to enhanced cellular chemotherapy uptake. However, observations of improved BMV blood flow and improved cellular uptake of chemotherapy do not assure increased extracellular drug accumulation after radiation therapy, because cellular drug uptake also depends on the number of cells in the tissue and the affinity of cells to uptake drugs.[16] Additionally, in vivo measurements of cellular drug uptake are limited to single time-point measurements and do not have the ability to observe sustained longitudinal changes in drug accumulation after treatment. Therefore, longitudinal measurements of extracellular drug accumulation would be beneficial to assess the effectiveness of radiation therapy in conditioning the BMV for chemotherapy delivery to the extracellular bone marrow.

We have developed longitudinal quantitative multiphoton microscopy (L-QMPM) to (1) directly assess extracellular drug accumulation and changes in the BMV after radiation therapy, (2) quantify potential time-lapsed imaging-based disease biomarkers, and (3) better understand the relationship between underlying vascular alterations and measurements obtained from DCE imaging. We quantified extracellular drug accumulation primarily as the extravascular tissue wash-in slope (WIS_{tissue}) calculated using time-lapsed imaging of 4 kDa dextran. We measured several additional time-lapsed imaging and microvascular parameters, including the kinetic transfer rate (K_{trans}) and single-vessel blood flow to understand how the BMV influences changes in DCE imaging parameters and WIS_{tissue}. We performed L-QMPM imaging in the calvarium of mice bearing ALL or AML, 2 common types of leukemia, as well as wild-type (WT) controls, to assess the response of the healthy and leukemic BMV to radiation therapy. We hypothesized that radiation therapy would increase WIS_{tissue} in the calvarium bone marrow of mice bearing leukemia after both low (2 Gy) and high (10 Gy) dose total body irradiation (TBI). After seeing the response of the BMV to 2 Gy and 10 Gy TBI we performed additional L-QMPM imaging on mice bearing ALL, which received 4 Gy TBI in a single treatment or in 2 treatments (4 Gy split-dose) to see how different nonmyeloablative treatments would affect extracellular drug accumulation.

Methods and Materials

Mice and cell lines

We performed all procedures for animal experimentation according to City of Hope guidelines and with approval from the Institutional Animal Care and Use Committee. For all imaging studies, we used male and female C57BL/6 WT mice (strain 556; Charles River, Wilmington, MA) at 7 to 11 weeks. Mice were injected with 1×10^6 green fluorescent protein$^+$ BCR-ABL (p190Kd) expressing B-cell ALL cells[17] or 1×10^6 green fluorescent protein$^+$ *Cbfb-MYH11/Mpl*$^+$ AML cells.[18] The percentage of leukemia in peripheral blood (PB) and in bone samples was measured by flow cytometry as described previously.[12] Complete details of the mice and leukemia injections can be found in Appendix E1A.

Cranial window surgery

Briefly, we anesthetized mice using 1.3% isoflurane and made an incision to expose the calvarium. A custom head plate made of carbon fiber or titanium for stereotactic viewing of the calvarium and a round glass coverslip were adhered to the calvarium using a combination of adhesives. Complete details of the surgery can be found in Appendix E1B.

L-QMPM image acquisition and analysis

For L-QMPM imaging, we anesthetized mice using 1.3% isoflurane. The cranial window head plate attached to the mouse was inserted into a stereotactic heated stage for imaging using a Prairie Ultima multiphoton microscope (Bruker Corporation, Billica, MA). We performed imaging on the frontal bone region of the calvarium, near the sagittal suture for all mice. For time-lapsed contrast imaging, we inserted a catheter into the tail vein of the mice[19] and injected 4 kDa tetramethylrhodamine-isothiocyanate dextran (TdB Consultancy, Uppsala, Sweden) 30 seconds after the start of time lapsed imaging. After completing time-lapsed imaging, a second injection of 2 MDa fluorescein isothiocyanate dextran (TdB Consultancy) or Qtracker 655 Vascular Label (Invitrogen, Carlsbad, CA) was performed to observe the vasculature morphology and identify vascular tissue. We used 3 separate z-stack images to measure vessel density and mean vessel diameter for each mouse using Fiji/ImageJ.[20] Measurements of corrected single-vessel blood flow were acquired as described previously.[4] Tiled z-stack images were stitched together using a Fiji/ImageJ plugin.[21] A complete description of image acquisition can be found in Appendix E1C.

For identification of extravascular, vascular, and whole tissue regions of interest (ROI), we performed a series of automatic thresholds from fluorescent blood pool agents and time-lapsed 4 kDa dextran images using Otsu's method[22] in Fiji/ImageJ in similar fashion to our previous work.[12] The average fluorescent intensity measurements from the 3 preinjection background frames were subtracted from the time-lapsed image data set for each ROI. Time-lapsed dextran accumulation in the vascular and extravascular tissue ROIs was analyzed using a custom MATLAB (R2018a 9.41.0.81364; MathWorks, Natick, MA) script to obtain K_{trans}, the fractional extracellular extravascular space (ν_{ec}), and the backflux rate (K_{ep}) using a 2-compartment model[23] as described in our previous work.[12] The additional parameters of dextran accumulation that we quantified included WIS_{tissue}, wash-in slope for the whole tissue ROI (WIS_{whole}), peak height for the extravascular tissue ROI (PH_{tissue}),

peak height for the whole tissue ROI (PH_{whole}), and peak height for the vascular tissue ROI (PH_{blood}). WIS_{whole} and PH_{whole} were quantified as measurements similar to DCE imaging parameters to identify how signal contributions from the vascular and extravascular tissue influence DCE imaging.[9]

We obtained WIS_{tissue} and WIS_{whole} by dividing the largest positive change in fluorescent intensity between each frame by the time interval between frames for the ROIs of the extravascular and whole tissues, respectively. PH_{blood}, PH_{tissue}, and PH_{whole} were calculated by measuring the dextran fluorescent intensity value of the frame with the highest fluorescent intensity for vascular, extravascular, and whole tissue ROIs, respectively[8] (Fig. 1A,B). A complete description of image segmentation, compartmental modeling, and descriptive curve analysis is found in the Appendix E1D.

TBI treatments, head plate dosimetry, and dose simulations

We used the Precision X-RAD SMART Plus/225cx small animal image guided irradiation system (Precision X-Ray, North Branford, CT)[24] to administer single-dose, soft tissue equivalent TBI treatments at 2, 4,or 10 Gy. Additionally, a 4 Gy split-dose TBI treatment consisting of 2 2 Gy TBI treatments separated by 3 days was performed. The system was also used to acquire CT images and perform dose calculations.[25,26] Further description of treatment and dosimetric evaluation can be found in Appendix E1E.

Histology preparation and scoring

Details of histology preparation can be found in Appendix E1F.

Statistical analysis

We performed all statistical testing using Prism (V.9.00 [121], GraphPad). For analysis of the treatment effects, a 2-way mixed-effects model was performed followed by Tukey's post hoc comparison when appropriate. For experiments using 2 and 10 Gy TBI, we performed post hoc comparisons with 3 families and 3 comparisons per family for both time and treatment group comparisons. Measurements of leukemia in the PB of mice in treatment groups were compared using a 1-way mixed-effect model for cross group and longitudinal comparisons. When appropriate, 4-Gy single-dose and 4-Gy split-dose TBI-treated mice were compared using a Welch's 2-sided *t* test corrected for multiple comparisons. Unless stated otherwise, we performed all other significance testing using a Welch's 2-sided *t* test. All distribution error bars are displayed as the mean ± 1 standard deviation.

Results

Study timing and L-QMPM validation

We performed treatment intervention for mice bearing AML and ALL approximately when the percentage of leukemia in the PB reached the level where changes in BMV function were observed (Fig. 1C,D, Tables E1 and E2). An additional group of mice bearing ALL were treated at higher ALL burden to observe the effects of TBI after ALL had caused significant reductions in WIS_{tissue} (Table E3).

To understand the differences between the timing of single-vessel blood flow changes in mice bearing AML or ALL, we characterized the growth kinetics of leukemia in the PB, femur, and calvarium. No significant time-matched differences in the percentage of leukemia in the PB of mice were found between mice bearing ALL and AML post leukemia-cell injection (Fig. E1A). However, in the calvarium, we observed significantly higher engraftment of ALL compared with AML (Fig. E1B,C). Similar differences were found in the femur bone marrow (Fig. E1C,D). The data suggest that differences in vascular function may be due to differences in the onset of leukemia engraftment in the calvarium and femur bone marrow.

We observed no significant differences in any imaging parameters in WT untreated mice between imaging time points (Table E4). Additionally, no significant differences in any of the imaging parameters or leukemia PB measurements were observed before TBI treatments in treatment subgroups with matching types of disease, validating longitudinal and cross-group comparisons posttreatment (Table E1–2). Leukemia growth and treatment response could be observed in the calvarium using L-QMPM (Figs. 1E–I and E2).

We performed dosimetry measurements at different regions underneath titanium and carbon fiber head plates and performed CT-based dose simulations to ensure accurate dose delivery and dose evaluation of the calvarium after cranial window surgery, respectively. Significant differences in dose were noticed between a lack of head plate and directly under the titanium head plate material, whereas no significant differences were noticed between a lack of head plate and carbon fiber headplates (Fig. 1J–L). We observed significant artifacts in CT images of mice with titanium head plates. However, no artifacts were present for carbon fiber head plates (Fig. 1M). For these reasons, we used carbon fiber head plates for all L-QMPM imaging studies.

AML and ALL increased vessel density, reduced blood flow, and reduced WIS_{tissue}

We split L-QMPM imaging data into relative low and high leukemic burden groups using PB measurements based on the timing of BMV changes. Reduced vascular diameter, increased vessel density, and reduced single-vessel blood flow were observed in mice bearing leukemia at both low and high leukemic burden compared with WT mice (Fig. 2A–D, Table E5).

BMV changes at low disease burden coincided with decreased WIS_{whole} for mice bearing leukemia compared with WT mice ($P = .0178$ and $P = .0018$; Fig. 2E, Table E5). We observed decreases in K_{ep} and increases in v_{ec} in mice bearing AML at low leukemic burden compared with WT mice ($P < .0001$ and $P = .0412$, respectively; Table E5).

At high leukemic burden, we observed decreases in WIS_{tissue} for mice bearing ALL and AML compared with WT mice ($P = .0001$ and $P = .0001$, respectively; Fig. 2F–G, Table E5). Significant differences for time-lapsed imaging parameters in mice bearing leukemia at high disease burden included decreased WIS_{tissue}, WIS_{whole}, PH_{whole}, PH_{blood}, and K_{ep}, as well as increased v_{ec} compared with WT mice (Fig. 2E–G, Table E5). We additionally observed decreased K_{trans} at high AML burden ($P < .0001$, Fig. 2H). The most effective

time-lapsed imaging parameter to distinguish between mice bearing leukemia and WT mice was WIS_{whole} (Figs. 2I–L and E3).

We measured the percent signal contribution to PH_{whole} from the extravascular tissue ROI, to better understand peak height measurements in DCE imaging. Mean signal contribution was 55.7% ± 16.7%, 64.9% ± 3.7%, and 71.7% ± 20.7% for untreated WT mice and mice bearing ALL or AML, respectively (Fig. E4A). We observed no correlation between PH_{whole} and vascular density using data from untreated WT mice and mice bearing AML and ALL ($R^2 = 0.005$, $P = .5235$; Fig. E4B).

2 and 10 Gy TBI reduced vascular density, dilated blood vessels, and, in mice bearing leukemia, increased blood perfusion

We observed accumulation of the macromolecular blood pool agent (Qtracker™ 655 vascular label) in large, tiled images of mice bearing ALL 2 days after treatment, suggesting increased vascular leakage and increased extracellular tissue space compared with pretreatment (Fig. 3A). Increases in mean vessel diameter were observed for all mice 2 days after 2 and 10 Gy TBI as well as 5 days after 10 Gy TBI compared with that in pretreatment time points and untreated mice (Fig. 3A,B, Tables E1–E4). For mice bearing AML or ALL, we observed increases in single-vessel blood flow 2 days after 2 Gy TBI and 10 Gy TBI compared with levels in pretreatment time points and untreated mice. Compared with untreated mice, increases in single-vessel blood flow were observed 5 days after 10 Gy TBI treatments for mice bearing leukemia (Fig. 3C, Tables E1 and E2).

For mice with leukemia, we observed decreases in vessel density 2 days after 10 Gy TBI compared with pretreatment density; for mice bearing ALL, we observed decreases compared with untreated mice (Fig. E4C). Decreases in vessel density were also observed 5 days after 10 Gy TBI for all mice, compared with levels in pretreatment time points and untreated mice. Decreases in vessel density and increases in vessel diameter were also observed 5 days after 10 Gy TBI compared with 2 Gy for all mice. We observed similar changes in vessel diameter and vessel density measurements 5 days after treatment in femur and calvarium histology (Fig. E5A–D).

2 and 10 Gy TBI increased extracellular drug accumulation to the healthy and leukemic bone marrow

We observed increases in WIS_{tissue} for all mice 2 days after both 2 Gy TBI and 10 Gy TBI compared with either pretreatment time points or untreated mice (Fig. 4A–D, Table E1–4). Percent increases in WIS_{tissue} mean values ranged from 39% to 81% for WT mice and 139% to 227% for mice bearing leukemia compared with pretreatment. Similar increases posttreatment for K_{trans} and K_{ep} were observed (Fig. 4E, Table E1–4). We observed increases in WIS_{tissue} 5 days after 10 Gy TBI for mice bearing leukemia compared with untreated mice, and we observed increases for mice bearing ALL compared with pretreatment time points. We additionally observed significant increases in WIS_{tissue} 5 days after 10 Gy TBI compared with 2 Gy for mice bearing AML or ALL (mean percent increases of 165% and 188%, respectively). We found significant decreases in WIS_{tissue} before treatment intervention in mice bearing AML or mice bearing ALL treated with 10 Gy

at high disease burden compared with WT mice ($P = .0279$ and .0003, respectively; Fig. E6), demonstrating that increases in WIS_{tissue} after TBI occurred in healthy or leukemic bone marrow microenvironments. We observed increases in PH_{tissue} and ν_{ec} after TBI at a variety of doses and time points likely due to changes in cellularity (Table E1–4). Similar changes in ν_{ec} after TBI are observed in DCE imaging.[27]

A summary of the effects of TBI is shown in Figure 5A. We found positive linear correlations with WIS_{tissue} for single-vessel blood flow and mean vessel diameter, and no correlation was found for vessel density (Fig. 5B).

4 Gy split-dose TBI increased the duration of improved extracellular drug accumulation

After seeing increases in WIS_{tissue} 5 days after 10 Gy TBI but not 2 Gy TBI, we measured the effects of 2 additional non-myeloablative treatments (4 Gy TBI and 4 Gy split-dose TBI) (Fig. 6A). These treatments were performed to see whether different nonmyeloablative treatments could extend the duration of improved extracellular drug accumulation compared with 2 Gy TBI. Four Gy split-dose TBI resulted in significant increases in WIS_{tissue} and K_{trans} at day 5 compared with pretreatment ($P = .0150$ and $P = .0003$ respectively), and no significant increases were seen for 2 Gy or 4 Gy treated mice (Fig. 6B,C). However, 4 Gy TBI significantly increased WIS_{tissue} at day 2 compared with 4 Gy split-dose TBI. Similar increases in mean vessel diameter and single-vessel blood flow at day 5 were observed for 4 Gy split-dose TBI (Fig. 6D–G). Data suggest that 4 Gy split-dose TBI extends the window of improved vascular function to at least 5 days after the start of treatment; however, 4 Gy single-dose TBI may provide further improved extracellular drug accumulation for a shorter duration.

Discussion

We developed L-QMPM imaging to measure several parameters that quantified the BMV and extracellular drug accumulation before and after radiation therapy. Decreased WIS_{tissue}, WIS_{whole}, PH_{whole}, K_{ep}, single-vessel blood flow, and mean vessel diameter, as well as increased vessel density and ν_{ec} were observed with the onset of leukemia. WIS_{whole} was the most effective contrast-based, time-lapsed imaging parameter to identify mice bearing leukemia. As hypothesized, 2 Gy and 10 Gy TBI treatments increased WIS_{tissue}, K_{trans}, and mean vessel diameter in WT mice and mice bearing leukemia 2 days after TBI. We also observed increased single-vessel blood flow for mice bearing AML and ALL. Increases in WIS_{tissue} were observed 5 days after 10 Gy myeloablative TBI and 2 Gy nonmyeloablative TBI caused no changes. However, nonmyeloablative 4 Gy split-dose TBI treatments resulted in an extended time window (up to 5 days) for increased WIS_{tissue} compared with single-dose 4 or 2 Gy TBI. Data suggest that the appropriately designed non-myeloablative treatment can condition the BMV for improved drug transport to the bone marrow for a variety of dosing timeframes.

DCE imaging analysis applies mathematical models to or infers the BMV changes that influence the delivery of contrast agents. We calculated WIS_{whole} and PH_{whole} as measurements commonly interpreted as the volumetric tissue blood flow rate and tissue blood volume for DCE imaging, respectively.[8] Several studies using DCE imaging

identified changes in PH_{whole} or similar mathematically modeled parameters to be positively correlated with vessel density and have proposed DCE imaging as an alternative method to quantify vessel density in the untreated malignant bone marrow.[10,28] This circumstance is desirable as it would reduce the need for invasive bone marrow biopsies to quantify vessel density, which is a prognostic marker for tumor aggressiveness.[29] However, in this work, we found no correlation between PH_{whole} and vessel density with leukemia onset, likely due to the reduction in mean vessel diameter present in mice bearing leukemia. Additionally, over half of the fluorescent signal contributing to PH_{whole} was from the extravascular ROI, suggesting that PH_{whole} measurements may be significantly influenced by leakage of contrast into the extravascular tissue. Our results demonstrate that positive correlations of PH_{whole} with vessel density or vessel volume cannot be assumed without pathologic validation, and that mathematical modeling should be used to account for signal contributions from the extravascular tissue when quantifying vascular parameters using DCE.

We identified WIS_{whole} as the most effective time-lapsed imaging measurement to identify mice bearing leukemia. As WIS_{whole} is primarily a measurement of volumetric blood flow, it will be closely related to mean vessel diameter, vessel density, and single-vessel blood flow, which are all affected early in leukemia progression. This enables WIS_{whole} to better identify mice bearing leukemia than other contrast-based time-lapsed imaging parameters that are less sensitive to early vascular alterations.

Because WIS_{whole} is primarily a measurement of volumetric blood flow, it is enticing to infer improved extracellular drug accumulation when increases in WIS_{whole} are observed. However, we observed that changes in WIS_{whole} and WIS_{tissue} did not occur at the same disease burden. Additionally, changes in WIS_{tissue} were observed in WT mice after TBI, but no changes were observed in WIS_{whole}. Our results demonstrated that WIS_{whole} may not accurately identify changes in extracellular drug accumulation, likely because WIS_{whole} is a convolution of signals from vascular and extravascular tissues. These observations identified the importance of validating extracellular drug accumulation when changes in DCE imaging parameters are observed.

Increases in WIS_{tissue} 2 days after TBI in WT mice were accompanied only by increases in K_{trans} and mean vessel diameter, suggesting that increases in WIS_{tissue} were due to increased vascular permeability or increases in vascular surface area, which commonly influence K_{trans}.[23] Similar alterations in K_{trans} after TBI have been observed previously using DCE-MRI.[27] For mice bearing leukemia, increases in blood flow after TBI may also contribute to increased WIS_{tissue}. Similar observations of improved tissue drug perfusion after radiation therapy have been made in solid tumor models,[30,31] suggesting that the leukemic BMV and solid tumor vasculature may have similar responses to radiation therapy. Our results suggest that increased WIS_{tissue} may be found after myeloablative and nonmyeloablative TBI treatments. This directly demonstrates the role of the BMV in our previous work, which observed increased cellular chemotherapy uptake by ALL cells and increased mouse survival after neoadjuvant radiation therapy.[12]

Although we observed similar changes in WIS_{tissue} 2 days after 2 and 10 Gy TBI, the duration of their changes was different. This finding suggests that the window of opportunity for synergistic combination therapy with therapeutics after reduced-intensity TBI regimens may be smaller than with standard myeloablative regimens of TBI.[32] However, 4 Gy split-dose TBI caused extended increases in WIS_{tissue} compared with 2 Gy TBI. This suggests that successive treatments of TBI may extend the duration of improved extracellular drug accumulation and enable a large variety of possible combination treatment approaches. Targeted irradiation treatment to the bone marrow may also help improve extracellular drug accumulation in regions of high leukemic burden while minimizing potential off-target toxicities from therapeutic agents.

We observed significant changes in vessel density and vessel diameter 5 days after 10 Gy TBI compared with 2 days, and no significant differences were noticed in WIS_{tissue}. These data suggest that maximum BMV morphologic changes after TBI may occur later than the maximum increases in WIS_{tissue}. These findings are in agreement with other studies observing vasodilation and macromolecular contrast leakage 4 to 7 days after myeloablative doses.[33,34] Future studies should identify how long-term vascular damage after myeloablative TBI and bone marrow transplantation influence extracellular drug accumulation.

We observed decreases in vessel density 2 days after 10 Gy treatment for mice bearing leukemia but not for WT mice, suggesting that the leukemic BMV may have increased radiosensitivity. Newly formed immature vessels have been shown to be sensitive to radiation therapy,[35,36] and more mature vascular structures have been found after fractionated radiation therapy in solid tumors.[37] This suggests that the appropriate radiation therapy treatment may be able to preserve mature vessels, while eliminating newly formed vessels present from leukemia signaling. Synergistic effects have been observed with radiation therapy and vascular based therapeutic agents for solid tumors,[38] making combination therapy an attractive option for the treatment of leukemia. Future studies evaluating the effects of combination therapy using TBI and typical clinical chemotherapy regimens should be performed to understand how radiation therapy can be used to improve the efficacy of existing clinical induction chemotherapy.

Although L-QMPM is useful to accurately assess extracellular drug accumulation, it is limited to preclinical models, making DCE imaging modalities such as MRI or CT necessary for clinical translation. In this work, we provide direct observations of BMV morphology and function, as well as measurements used in DCE imaging. These observations will be invaluable for interpretation of DCE imaging of the bone marrow.

Conclusions

We identified WIS_{whole} as the most effective DCE imaging parameter to distinguish between WT mice and mice bearing AML or ALL. This suggests that DCE imaging should focus on the rate of initial increase in whole tissue contrast signal during time-lapsed imaging as a biomarker for leukemia. Our results show that the response of the leukemic BMV to neoadjuvant radiation therapy at nonmyeloablative and myeloablative doses improves

extracellular drug accumulation in the bone marrow by improving blood flow and increasing drug permeation through the BMV to the extravascular tissue.

Supplementary Material

Refer to Web version on PubMed Central for supplementary material.

Acknowledgments

Research reported in this publication is supported by the National Cancer Institute of the National Institutes of Health under (P30CA033572) and partly supported by National Institutes of Health grant (2R01CA154491–01), ONCOTEST (Ghent, Belgium).

Disclosures: S.H. receives honoraria from and consults for Janssen Research & Development, LLC, outside of the submitted work. K.G. receives honoraria from and consults for Tautona Group, receives honoraria and is an advisory committee member for Novartis, reports grants from 1910 Genetics, reports grants from Grifols, receives honoraria from CSL Behring, LLC, and reports grants from Cyclerion outside of the submitted work. All other authors report no conflict of interest.

References

1. Passaro D, Di Tullio A, Abarrategi A, et al. Increased vascular permeability in the bone marrow microenvironment contributes to disease progression and drug response in acute myeloid leukemia. Cancer Cell 2017;32 324–341.e6.
2. Duarte D, Hawkins ED, Akinduro O, et al. Inhibition of endosteal vascular niche remodeling rescues hematopoietic stem cell loss in AML. Cell Stem Cell 2017;22:64–77.e6. [PubMed: 29276143]
3. Hussong JW, Rodgers GM, Shami PJ. Evidence of increased angiogenesis in patients with acute myeloid leukemia. Blood 2000;95:309–313. [PubMed: 10607717]
4. Schaefer C, Krause M, Fuhrhop I, et al. Time-course-dependent microvascular alterations in a model of myeloid leukemia in vivo. Leukemia 2007;22:59. [PubMed: 17898789]
5. Ossenkoppele GJ, Stussi G, Maertens J, et al. Addition of bevacizumab to chemotherapy in acute myeloid leukemia at older age: A randomized phase 2 trial of the Dutch-Belgian Cooperative Trial Group for Hemato-Oncology (HOVON) and the Swiss Group For Clinical Cancer Research (SAKK). Blood 2012;120:4706–4711. [PubMed: 23047822]
6. Jain P, Lee HJ, Qiao W, et al. FCR and bevacizumab treatment in patients with relapsed chronic lymphocytic leukemia. Cancer 2014;120:3494–3501. [PubMed: 25043749]
7. Haibe Y, Kreidieh M, El Hajj H, et al. Resistance mechanisms to anti-angiogenic therapies in cancer. Front Oncol 2020;10:221. [PubMed: 32175278]
8. Cuenod CA, Balvay D. Perfusion and vascular permeability: Basic concepts and measurement in DCE-CT and DCE-MRI. Diag Intervent Imaging 2013;94:1187–1204.
9. Faye N, Fournier L, Balvay D, et al. Dynamic contrast enhanced optical imaging of capillary leakage. Tech Cancer Res Treat 2011;10:49–57.
10. Shih TTF, Tien HF, Liu CY, et al. Functional MR imaging of tumor angiogenesis predicts outcome of patients with acute myeloid leukemia. Leukemia 2006;20:357–362. [PubMed: 16357837]
11. Petrakis NL, Masouredis SP, Miller P, et al. The local blood flow in human bone marrow in leukemia and neoplastic diseases as determined by the clearance rate of radioiodide (I131). J Clin Invest 1953;32:952–963. [PubMed: 13096561]
12. Brooks J, Kumar B, Zuro DM, et al. Biophysical characterization of the leukemic bone marrow vasculature reveals benefits of neoadjuvant low-dose radiation therapy. Int J Radiat Oncol Biol Phys 2021;109:60–72. [PubMed: 32841681]
13. Jung Y, Spencer JA, Raphael AP, et al. Intravital imaging of mouse bone marrow: Hemodynamics and vascular permeability. In: Ishii M, ed. Intravital Imaging of Dynamic Bone and Immune Systems: Methods and Protocols. New York, NY: Springer New York; 2018:11–22.

14. Dombret H, Gardin C. An update of current treatments for adult acute myeloid leukemia. Blood 2016;127:53–61. [PubMed: 26660429]
15. Pustylnikov S, Sagar D, Jain P, et al. Targeting the C-type lectins-mediated host-pathogen interactions with dextran. J Pharm Pharm Sci 2014;17:371–392. [PubMed: 25224349]
16. Dewhirst MW, Secomb TW. Transport of drugs from blood vessels to tumour tissue. Nat Rev Cancer 2017;17:738–750. [PubMed: 29123246]
17. Manlove LS, Berquam-Vrieze KE, Pauken KE, et al. Adaptive immunity to leukemia is inhibited by cross-reactive induced regulatory T cells. J Immunol 2015;195:4028–4037. [PubMed: 26378075]
18. Hossain DMS, Dos Santos C, Zhang Q, et al. Leukemia cell−targeted STAT3 silencing and TLR9 triggering generate systemic antitumor immunity. Blood 2014;123:15–25. [PubMed: 24169824]
19. Egawa G, Ono S, Kabashima K. Intravital imaging of vascular permeability by two-photon microscopy. In: Nagamoto-Combs K, ed. Animal Models of Allergic Disease: Methods and Protocols. New York, NY: Springer US; 2021:151–157.
20. Schindelin J, Arganda-Carreras I, Frise E, et al. Fiji: An open-source platform for biological-image analysis. Nat Meth 2012;9:676.
21. Preibisch S, Saalfeld S, Tomancak P. Globally optimal stitching of tiled 3D microscopic image acquisitions. Bioinformatics 2009;25:1463–1465. [PubMed: 19346324]
22. Otsu N. A threshold selection method from gray-level histograms. IEEE Trans Syst, Man, Cybernet 1979;9:62–66.
23. Tofts PS. Modeling tracer kinetics in dynamic Gd-DTPA MR imaging. J Magn Res Imag 1997;7:91–101.
24. van Hoof SJ, Granton PV, Verhaegen F. Development and validation of a treatment planning system for small animal radiotherapy: Smartplan. Radiother Oncol 2013;109:361–366. [PubMed: 24183860]
25. Faddegon BA, Kawrakow I, Kubyshin Y, et al. The accuracy of EGSnrc, Geant4 and PENELOPE Monte Carlo systems for the simulation of electron scatter in external beam radiotherapy. Phys Med Biol 2009;54:6151–6163. [PubMed: 19779217]
26. Downes P, Jarvis R, Radu E, et al. Monte Carlo simulation and patient dosimetry for a kilovoltage cone-beam CT unit. Med Phys 2009;36:4156–4167. [PubMed: 19810489]
27. Wang K, Zha Y, Lei H, et al. MRI study on the changes of bone marrow microvascular permeability and fat content after total-body x-ray irradiation. Radiat Res 2018;189:205–212. [PubMed: 29251550]
28. Moehler TM, Hawighorst H, Neben K, et al. Bone marrow microcirculation analysis in multiple myeloma by contrast-enhanced dynamic magnetic resonance imaging. Int J Cancer 2001;93:862–868. [PubMed: 11519049]
29. Hlatky L, Hahnfeldt P, Folkman J. Clinical application of antiangiogenic therapy: Microvessel density, what it does and doesn't tell us. J Natl Cancer Inst 2002;94:883–893. [PubMed: 12072542]
30. Potiron VA, Abderrahmani R, Clément-Colmou K, et al. Improved functionality of the vasculature during conventionally fractionated radiation therapy of prostate cancer. PloS One 2013;8:e84076.
31. Kleibeuker EA, Fokas E, Allen PD, et al. Low dose angiostatic treatment counteracts radiotherapy-induced tumor perfusion and enhances the anti-tumor effect. Oncotarget 2016;7:76613–76627.
32. Gyurkocza B, Sandmaier BM. Conditioning regimens for hematopoietic cell transplantation: One size does not fit all. Blood 2014;124:344–353. [PubMed: 24914142]
33. Le V-H, Lee S, Lee S, et al. In vivo longitudinal visualization of bone marrow engraftment process in mouse calvaria using two-photon microscopy. Sci Rep 2017;7:44097. [PubMed: 28276477]
34. Slayton WB, Li X-M, Butler J, et al. The role of the donor in the repair of the marrow vascular niche following hematopoietic stem cell transplant. Stem Cells 2007;25:2945–2955. [PubMed: 17656638]
35. Grabham P, Hu B, Sharma P, et al. Effects of ionizing radiation on three-dimensional human vessel models: Differential effects according to radiation quality and cellular development. Radiat Res 2011;175:21–28. [PubMed: 21175343]

36. Park M-T, Oh E-T, Song M-J, et al. The radiosensitivity of endothelial cells isolated from human breast cancer and normal tissue in vitro. Microvasc Res 2012;84:140–148. [PubMed: 22705362]

37. Chen F-H, Fu S-Y, Yang Y-C, et al. Combination of vessel-targeting agents and fractionated radiation therapy: The role of the SDF-1/CXCR4 pathway. Int J Radiat Oncol Biol Phys 2013;86:777–784. [PubMed: 23601898]

38. Wachsberger P, Burd R, Dicker AP. Tumor response to ionizing radiation combined with antiangiogenesis or vascular targeting agents. Explor Mech Interact 2003;9:1957–1971.

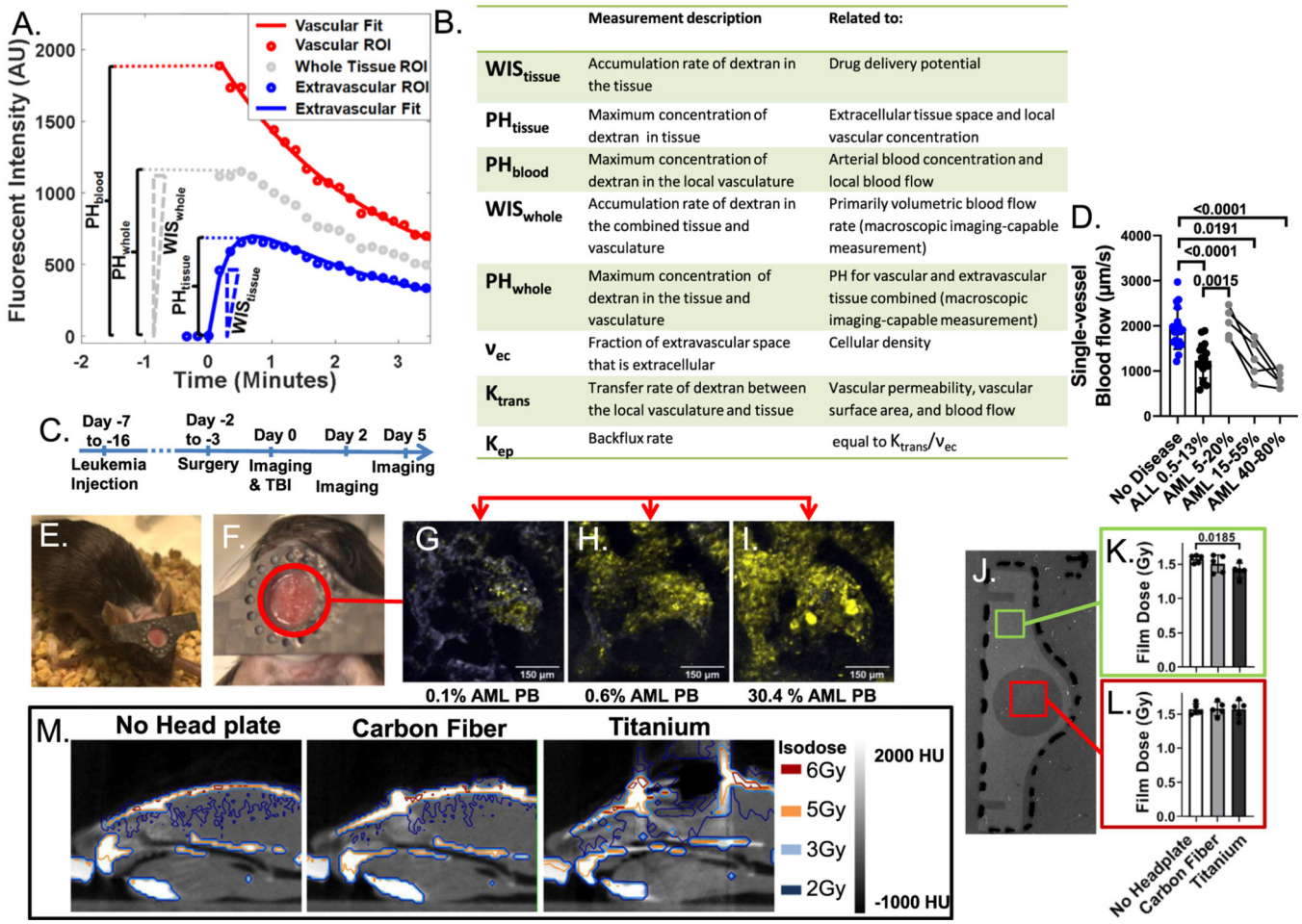

	Measurement description	Related to:
WIS_{tissue}	Accumulation rate of dextran in the tissue	Drug delivery potential
PH_{tissue}	Maximum concentration of dextran in tissue	Extracellular tissue space and local vascular concentration
PH_{blood}	Maximum concentration of dextran in the local vasculature	Arterial blood concentration and local blood flow
WIS_{whole}	Accumulation rate of dextran in the combined tissue and vasculature	Primarily volumetric blood flow rate (macroscopic imaging-capable measurement)
PH_{whole}	Maximum concentration of dextran in the tissue and vasculature	PH for vascular and extravascular tissue combined (macroscopic imaging-capable measurement)
v_{ec}	Fraction of extravascular space that is extracellular	Cellular density
K_{trans}	Transfer rate of dextran between the local vasculature and tissue	Vascular permeability, vascular surface area, and blood flow
K_{ep}	Backflux rate	equal to K_{trans}/v_{ec}

Fig. 1.

Time-lapsed imaging parameters and validation of longitudinal cranial window head plates. (A) Fluorescent intensity values from extravascular tissue, vascular tissue, and whole tissue regions of interest (ROIs) from time-lapsed longitudinal quantitative multiphoton microscopy (L-QMPM) images during the injection of 4 kDa tetramethylrhodamine-isothiocyanate (TRITC) dextran. Three background frames are taken before the injection of contrast to calculate the average background fluorescent intensity for the vascular, extravascular, and whole tissue ROIs. The average background fluorescent intensities are subtracted from the respective time-lapsed fluorescent intensity data. Solid lines represent fitted functions for the vascular and extravascular tissue compartments used to obtain kinetic transfer rate, backflux rate, and extracellular extravascular space. Wash-in slope and wash-in slope for the whole tissue ROI are depicted as the maximum positive slope between image frames for the extravascular tissue ROI and whole tissue ROI, respectively. (B) A summary of imaging parameters used in this study. (C) The L-QMPM imaging schema. (D) Single-vessel blood flow values for wild-type mice and mice with varying percentages of leukemia in peripheral blood. Mice bearing acute lymphoblastic leukemia were imaged 7 to 8 days after acute lymphoblastic leukemia injection and mice bearing acute myeloid leukemia (AML) were imaged longitudinally 9, 11, and 14 days after AML injection. (E,F) Photos of mice with longitudinal cranial windows. L-QMPM images of green fluorescent

protein + AML cell growth (green) in the calvarium at (G) 4, (H) 6, and (I) 10 days post-AML injection shown with corresponding peripheral blood measurements. (J) A picture of dosimetric film after x-ray exposure while directly underneath a titanium head plate. Film dose measurements from a lack of head plate, carbon fiber head plates, and titanium head plates obtained both (K) underneath the head plate material and (L) in the imaging area. (M) Computed tomography images with corresponding isodose lines for mice with no head plate, carbon fiber head plate, and titanium head plate. *Abbreviations:* ALL = acute lymphoblastic leukemia; AML = acute myeloid leukemia; AU = arbitrary units; HU = hounsfield unit; K_{ep} = backflux rate; K_{trans} = kinetic transfer rate; PB = peripheral blood; PH_{blood} = peak height for the vascular tissue region of interest; PH_{tissue} = peak height for the extravascular tissue region of interest; PH_{whole} = peak height for the whole tissue region of interest; ROI = region of interest; TBI = total body irradiation; v_{ec} = extracellular extravascular space; WIS_{tissue} = wash-in slope; WIS_{whole} = wash-in slope for the whole tissue region of interest.

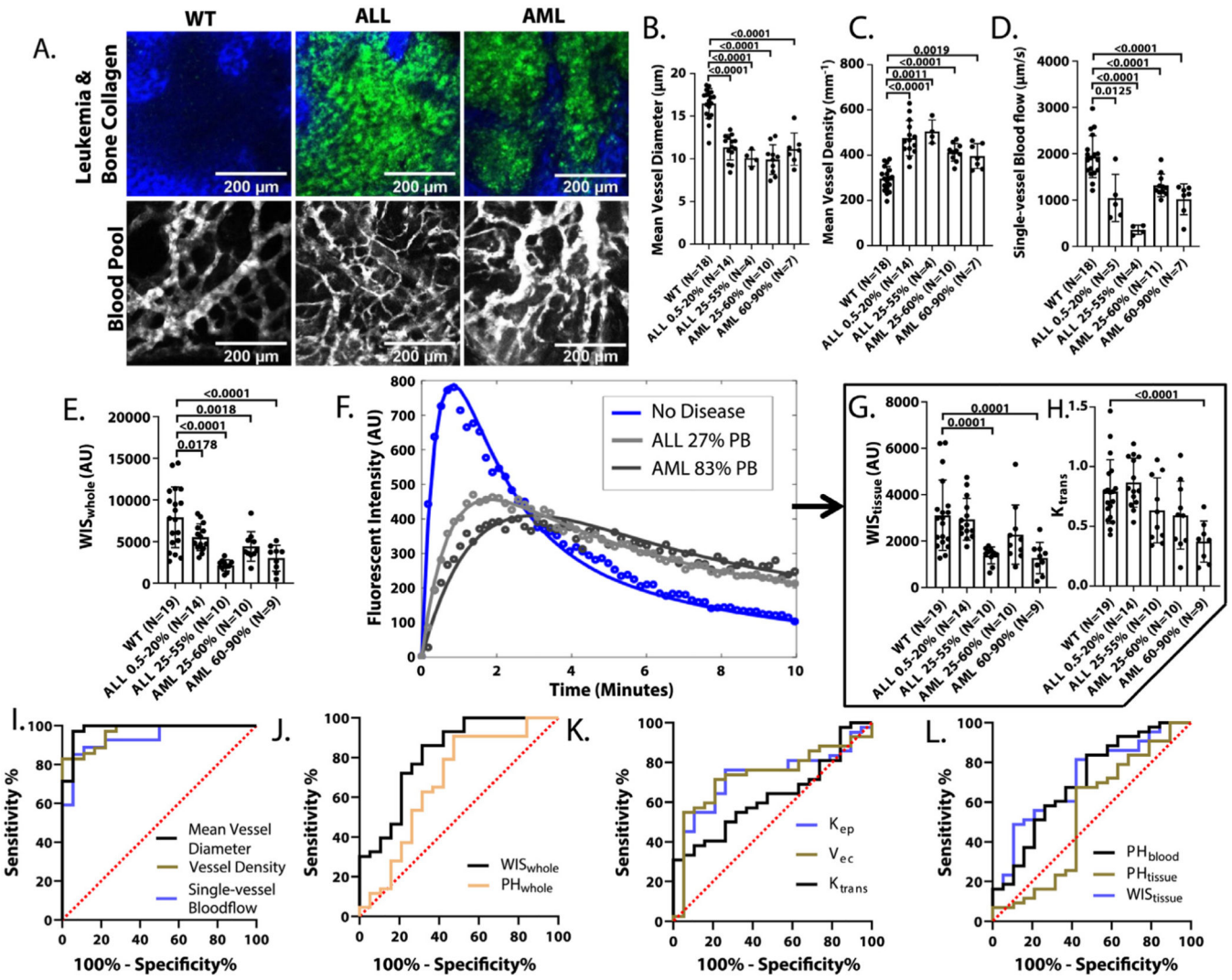

Fig. 2.

Bone marrow vasculature remodeling with the onset of leukemia. (A) Top: images of green fluorescent protein + leukemia (green) and second harmonic generation from the collagen in the bone (blue). Bottom: Images of bone marrow vasculature blood pool fluorescence from Qtracker™ 655 vascular labels (white). Longitudinal quantitative multiphoton microscopy measurements of (B) mean vessel diameter, (C) mean vessel density, (D) single-vessel blood flow, (E) wash-in slope for the whole tissue region of interest, (G) wash-in slope, and (H) kinetic transfer rate for wild-type mice and mice with varying leukemic burdens measured through peripheral blood sampling. (F) Four kDa dextran fluorescent intensity from extravascular tissue regions of interest from a wild-type mouse, mouse bearing acute lymphoblastic leukemia, and mouse bearing acute myeloid leukemia. Solid lines indicate the corresponding fitting function used for compartmental modeling. (I-L) Receiver operating characteristic curves for a variety of longitudinal quantitative multiphoton microscopy parameters. A single measurement time point from each mouse, typically matching the highest untreated disease burden, was used for analysis of all imaging parameters. *Abbreviations:* ALL = acute lymphoblastic leukemia; AML = acute myeloid leukemia; AU

= arbitrary units; K_{ep} = backflux rate; K_{trans} = kinetic transfer rate; PH_{blood} = peak height for the vascular tissue region of interest; PH_{tissue} = peak height for the extravascular tissue region of interest; PH_{whole} = peak height for the whole tissue region of interest; v_{ec} = extracellular extravascular space; WIS_{tissue} = wash-in slope; WIS_{whole} = wash-in slope for the whole tissue region of interest; WT = wild-type.

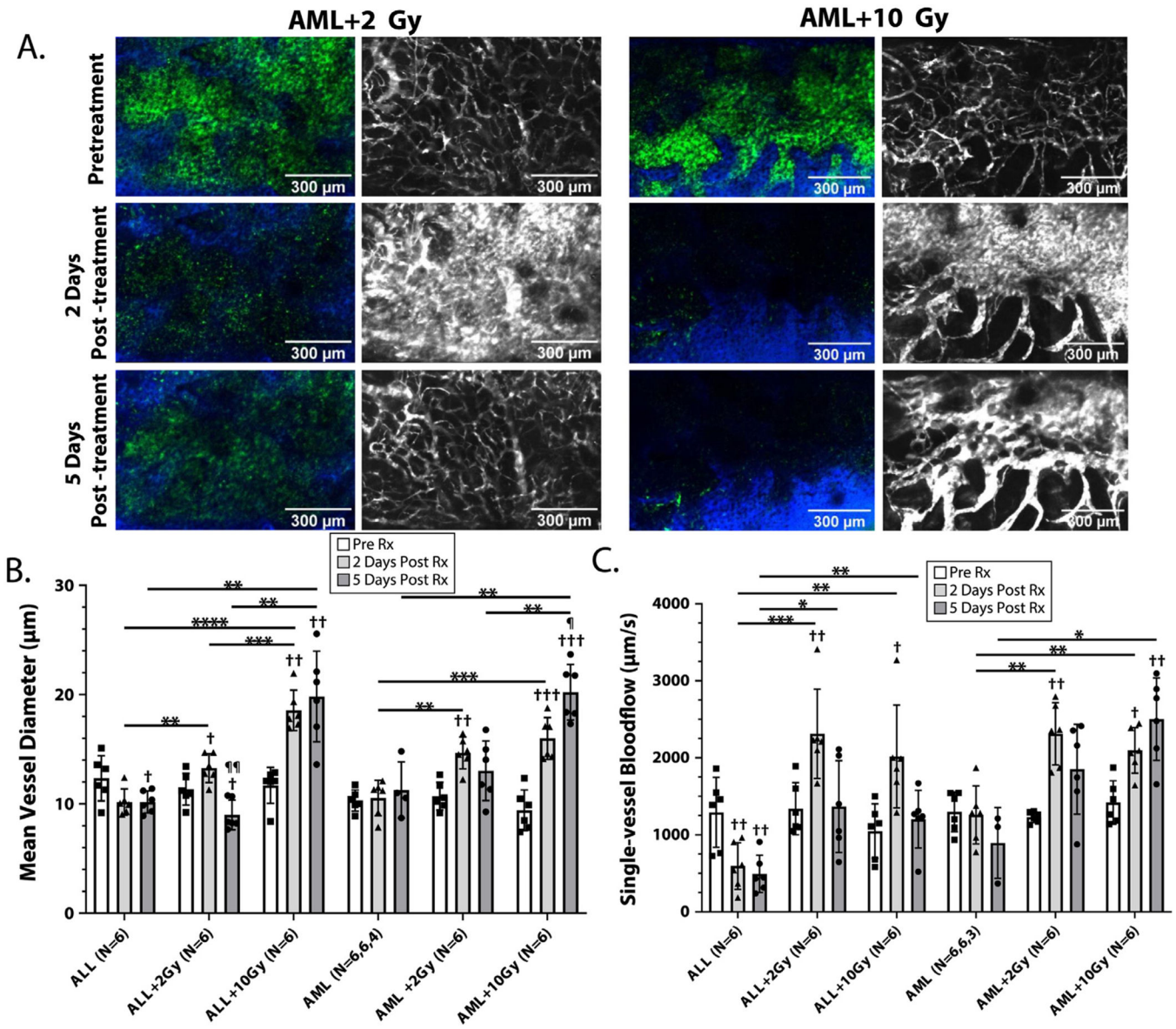

Fig. 3.

Total body irradiation (TBI) induced changes in leukemic burden, vascular leakiness, single-vessel blood flow, and vessel diameter. (A) Left: images of acute myeloid leukemia (AML) (green) and second harmonic generation from the collagen in the bone (blue). Right: maximum intensity projection images of Qtracker™ 655 vascular label (white). Images were acquired by stitching of 6 separate 3-dimensional z-stack images together. Stitched image sets took approximately 10 minutes to acquire and were started approximately 5 minutes after injection of Qtracker™ 655. Substantial vascular leakage and reduction in AML burden was observed 2 days after TBI. The effects of TBI on (B) mean vessel diameter and (C) single-vessel blood flow for mice bearing acute lymphoblastic leukemia and AML (*$P < .05$, ** $P < .01$, *** $P < .001$, **** $P < .0001$, compared with pretreatment time point: $^{\dagger}P < .05$, $^{\dagger\dagger}P < .01$, $^{\dagger\dagger\dagger}P < .001$, $^{\dagger\dagger\dagger\dagger}P < .0001$, compared with 2 days posttreatment time point:

¶$P < .05$, ¶¶$P < .01$, ¶¶¶$P < .001$, ¶¶¶¶$P < .0001$). *Abbreviations:* ALL = acute lymphoblastic leukemia; AML = acute myeloid leukemia; AU = arbitrary units; Rx = irradiation.

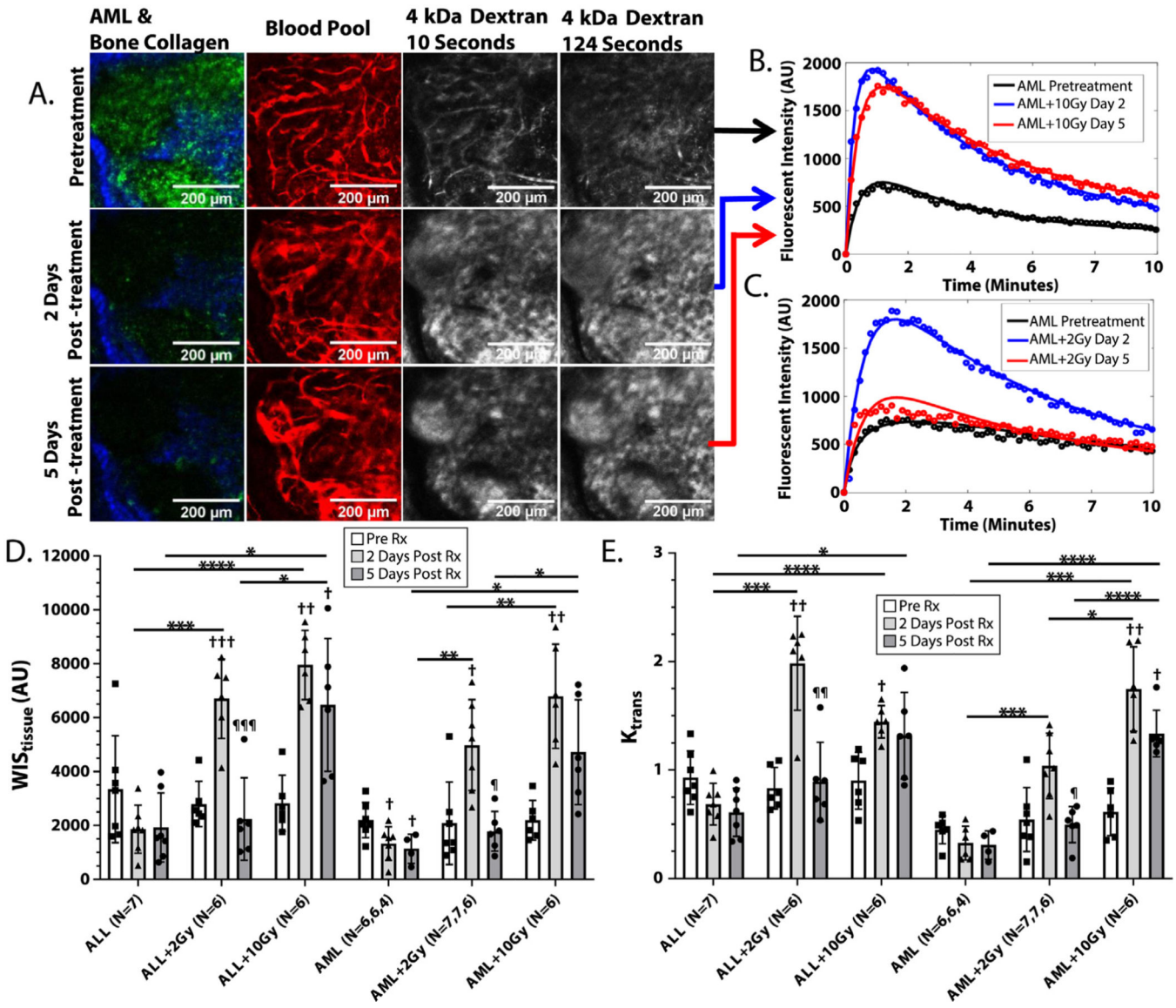

Fig. 4.

Measurements of bone marrow vasculature drug delivery potential. (A) Images of acute myeloid leukemia (green) and second harmonic generation from the collagen in the bone (blue) (far left). Images of 2 MDa fluorescein isothiocyanate (FITC) dextran vascular contrast (red) (left middle). Images of 4 kDa dextran (white) from the first frame after injection of dextran (right middle). Images of 4 kDa dextran (white) from the 12th frame after dextran injection (far right). A dose of 10 Gy total body irradiation (TBI) was given to the imaged mouse. Two MDa FITC dextran images were taken immediately after dextran injection before leakage into the extravascular tissue occurred. This enabled clear identification of the vascular structure and segmentation of the vascular tissue regions of interest (ROIs). (B) Fluorescent intensity values from the extravascular tissue ROI taken from time-lapsed images of 4 kDa dextran from the mouse images shown in Figure 4A. Solid lines indicate the extravascular fitting function for compartment modeling. (C) Fluorescent intensity values from the extravascular tissue ROI taken from a representative

mouse treated with 2 Gy TBI. The effects of TBI on (D) wash-in slope and (E) kinetic transfer rate for mice bearing acute lymphoblastic leukemia or acute myeloid leukemia. (* P < .05, ** P < .01, *** P < .001, **** P < .0001, compared with pretreatment time point: $^{\dagger}P$ < .05, $^{\dagger\dagger}P$ < .01, $^{\dagger\dagger\dagger}P$ < .001, $^{\dagger\dagger\dagger\dagger}P$ < .0001, compared with 2 days posttreatment time point: $^{\P}P$ < .05, $^{\P\P}P$ < .01, $^{\P\P\P}P$ < .001, $^{\P\P\P\P}P$ < .0001, Tukey's post hoc comparison.) *Abbreviations:* ALL = acute lymphoblastic leukemia; AML = acute myeloid leukemia; Rx = irradiation; WIS_{tissue} = wash-in slope.

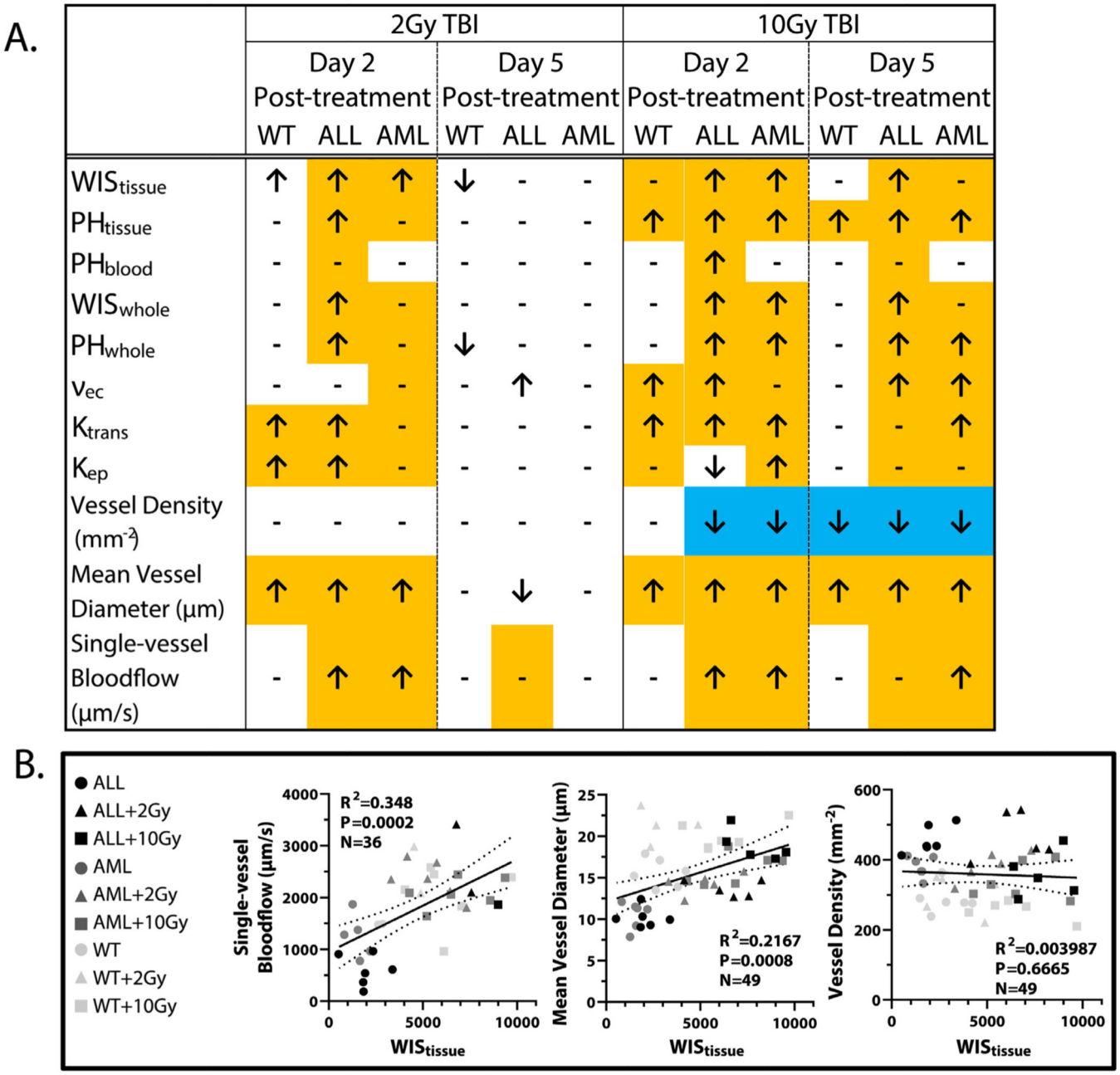

Fig. 5.

Summary of total body irradiation (TBI) treatment effects, and correlation to wash-in slope. (A) A summary of the response of wild-type mice and mice bearing acute lymphoblastic leukemia and acute myeloid leukemia to 2 and 10 Gy TBI treatments. Arrows indicate a significant increase or decrease compared with pretreatment time points, orange indicates a significant increase compared with the untreated group, and blue indicates a significant decrease compared with the untreated group ($P < .05$ for all). (B) Linear correlation plots for longitudinal quantitative multiphoton microscopy imaging parameters plotted with data from the time point 2 days after TBI treatments. A single image time point was used per mouse. *Abbreviations:* ALL = acute lymphoblastic leukemia; AML = acute myeloid leukemia; K_{ep}

= backflux rate; K_{trans} = kinetic transfer rate; PH_{blood} = peak height for the vascular tissue region of interest; PH_{tissue} = peak height for the extravascular tissue region of interest; TBI = total body irradiation; WIS_{tissue} = wash-in slope; WIS_{whole} = wash-in slope for the whole tissue region of interest; v_{ec} = extracellular extravascular space; WT = wild-type.

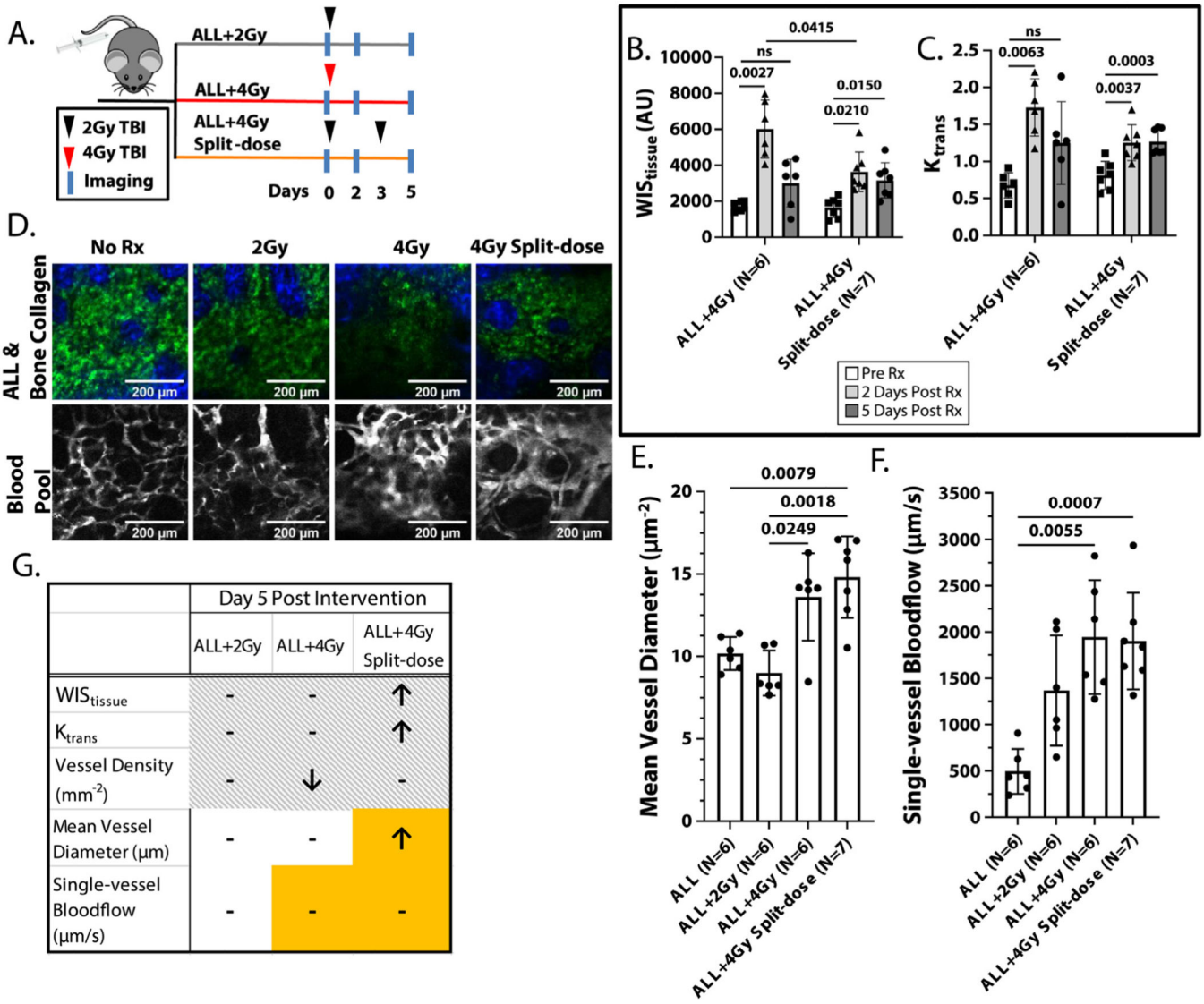

Fig. 6.

Treatment effects of nonmyeloablative total body irradiation (TBI) dose regimens for mice bearing acute lymphoblastic leukemia (ALL). (A) The treatment schema for mice bearing ALL and receiving 2 Gy TBI, 4 Gy TBI, and 4 Gy split-dose TBI. Measurements of (B) wash-in slope (WIS_{tissue}) and (C) kinetic transfer rate (K_{trans}) for mice bearing ALL receiving 4 Gy TBI and 4 Gy split-dose TBI before treatment, and on days 2 and 5 after the start of treatment. (D) Top: images of green fluorescent protein + leukemia (green) and second harmonic generation from the collagen in the bone (blue). Bottom: images of bone marrow vasculature blood pool fluorescence from 2 MDa fluorescein isothiocyanate (FITC) dextran immediately after injection (white). Images of treated mice were taken 5 days after the start of treatment. Measurements of (E) mean vessel diameter and (F) single-vessel blood flow 5 days after the start of treatment. (G) A summary of the effects of TBI treatment regimens 5 days after the start of treatment. Arrows indicate a significant increase or decrease compared with pretreatment time points, orange indicates a significant

increase compared with the untreated group, and the striped background indicates complete cross-group comparison was not appropriate owing to significant differences in pretreatment values between some groups ($P < .05$ for all). *Abbreviations:* ALL = acute lymphoblastic leukemia; AML = acute myeloid leukemia; K_{trans} = kinetic transfer rate; Rx = irradiation; TBI = total body irradiation; WIS_{tissue} = wash-in slope; WT = wild-type.